An Integrated Model of the Flight and Tether Dynamics of a Marine Hydrokinetic Energy Harvesting System

Miguel Alvarez, Debapriya Bhattacharjee, Chris Vermillion, and Hosam K. Fathy

***Abstract*— This paper models the dynamics of a marine tethered energy harvesting system focusing on exploring the sensitivity of the kite dynamics to tether parameters. These systems repetitively reels a kite out at high tension, then reels it in at low tension, in order to harvest energy. The kite's high lift-to-drag ratio makes it possible to maximize net energy output through periodic cross-current flight. Significant modeling efforts exist in the literature supporting such energy maximization. The goal of this paper is to address the need for a simple model capturing the interplay between the system's kite and tether dynamics. The authors pursue this goal by coupling a partial differential equation (PDE) model of tether dynamics with a point mass model of translational kite motion. One can simplify this model significantly by neglecting tether mass and compliance, effectively transforming the tether into a kinematic constraint. Simulation results show that the coupling effects discarded through such a simplification are non-trivial. For example, even when the tether is neutrally buoyant, its transverse vibrations can still cause significant oscillations in net kite forcing.**

I. Introduction

This paper models the coupled dynamics of the tether and kite used in a marine hydrokinetic energy harvester. Figure 1 provides a sketch of this harvester. Reeling the kite out under tension harvests energy. Ideally, the kite is reeled back in under much lower tether tension levels, so that only a fraction of the total energy harvested is reinvested in kite recovery. Tethered energy harvesters exploiting such "pumping" motion are under active exploration for both airborne and marine hydrokinetic applications. The practical appeal of such systems is twofold. First, substantial renewable energy resources exist at locations, altitudes, and depths beyond the affordable reach of traditional fixed infrastructure systems, such as fixed wind towers or water turbines. Tethered systems have the potential to harvest energy affordably from such hard-to-reach resources, such as high-altitude winds or Gulf Stream currents [1]. Second, a high lift-to-drag tethered system can maximize its energy harvesting potential through cross-current flight. This fact, highlighted in a seminal 1980 paper by Lloyd [2], serves as a key motivator for much of today's research on tethered energy harvesting.

There is a rich existing literature on the modeling, optimization, and control of tethered energy harvesting systems. Most of this literature focuses on airborne wind energy harvesting systems, with a growing interest in marine hydrokinetic systems. For both airborne and marine systems, the literature tends to model the tether in two ways: assuming the tether is rigid, or assuming it can deform. There are advantages and disadvantages to each approach. For instance, in the context of optimization, assuming a rigid tether decreases the number of optimization variables required and can make the optimization problem easier to solve. On the other hand, allowing the tether to deform may allow for a more accurate modeling of the system.

There are multiple examples of rigid tether in the literature. This is typically implemented in practice by imposing a kinematic constraint on the kite's position. For instance, Cobb et al. [3] used such a modeling approach. In their paper, they used iterative learning to optimize the path of a marine hydrokinetic system. For this, they modeled the kite as a three-dimensional unifoil with six degrees of freedom. They modeled the tether by constraining the kite to a sphere of radius equal to the tether length. One consequence of this approach is that it imposes that the tension force applied to the kite always points in the direction of the base station. This assumption is prevalent in the literature as it helps simplify the kite flight optimization problem. Another example of tethered marine harvester modeling, is the one proposed by Li et al. [4]. They also made the rigid tether assumption to explore the stability of the system and design an nonlinear controller to control the kite. We also find more examples of treating the tether as rigid in the airborne wind energy literature. Canale et al. [5], for example used model predictive control to maximize the energy generated by a kite with a rigid tether. Similarly, Costello et al. [6], used a simplified model which includes a rigid tether for optimization. William et al. [7] also assumed a straight tether for a kite towing a ground vehicle.

While the assumption of a rigid tether simplifies the optimal trajectory generation problem, it might miss some relevant dynamics. For example, allowing the kite to deform affects the kite dynamics by modifying the direction of the tension force. One way this is handled in the tethered kite literature, is by using a discrete lumped mass approximation to model the tether. In this approach the tether is discretized as a series of point masses. This masses can be elastically connected (with springs) or inelastically connected. For instance, Williams et al. [8] modeled the tether, for an airborne kite system, using inelastic links. Koenemann et al. [9] used a quasi-static tether approximation in the context of the optimal control of tether kites during landing maneuvers. This approach allowed them to neglect vibrations while still

Miguel Alvarez (malvarez@umd.edu) and Debapriya Bhattacharjee (dbhatta1@umd.edu) are Mechanical Engineering Ph.D. students at The University of Maryland, College Park, where Hosam K. Fathy (hfathy@umd.edu) serves as a professor of Mechanical Engineering.

Chris Vermillion (cvermil@ncsu.edu) is a professor of Mechanical & Aerospace Engineering at North Carolina State University

modeling the shape of the tether. Also for airborne wind energy systems, Trevisi et. al [10] proposed an approximate analytical approach to account for the effect of the tether sag on the power generation of the kite. While the literature for marine systems is more scarce than the airborne wind energy literature, there is still work that considers a tether using the lumped mass approach. For instance, Williams et al. [11] used the lumped mass tether model and compared it to experimental results. Similarly, Siddiqui et al. [12] compare a tethered underwater kite model that uses a lumped mass tether model with experimental results in a water channel.

Another way to model the tether is to describe its shape with a continuous, partial differential model. While this approach is not as common in the tethered energy generation literature, there is a body of tether systems literature particularly relevant. For instance, in 1983 Ablow and Schechter [13] simulated the dynamics of an undersea cable this way. Driscoll et al. [14] applied Galerkin methods to a continuous model of the tether of an underwater robot.

To design controllers that maximize the energy generated by tethered harvesters, we need simple dynamic models that can capture the relevant dynamics of these systems. It is thus critical to determine which dynamics are relevant and which dynamics can be negligible. While for tethered airborne wind energy the validity of rigid tethers has been explored [7], this has not been explored for tethered marine hydrokinetic systems.

In this paper we explore the effect the tether dynamics have on the kite. More specifically, we explore the effect of buoyancy, mass, and compliance of tether. A deeper examination of the tether fluid-structure interactions is beyond the scope of this paper. The main contributions in this paper are summarized here:

1) We propose a partial differential model for the dynamics of a tethered marine hydrokinetic energy harvester with a coordinate transformation that allows a simple handling of the moving boundary conditions of the tether PDE.
2) We explore the effect of a flexible tether model on the kite dynamics by coupling our tether model with a 3DOF kite model.
3) We explore the sensitivity of the combined tether/kite dynamics to tether parameters.

II. Kite Model

In the water, the kite experiences the following forces: gravitational forces, tension forces, buoyancy forces, and hydrodynamic surface forces. The hydrodynamic surface forces are typically decomposed into lift, drag, and side force.

We propose a simplified 3-degrees-of-freedom model for the kite. We assume that the rolling and pitch dynamics are faster than the translational dynamics of the center of mass, so that the kite can be represented as a point mass. Additionally, we assume the kite is buoyant, that is to say that the weight of the kite cancels with the buoyancy force. We also assume we control the kite's position by changing the angle of the lift vector with respect to a unit vector in the plane formed by the relative wind and position vector of the kite.

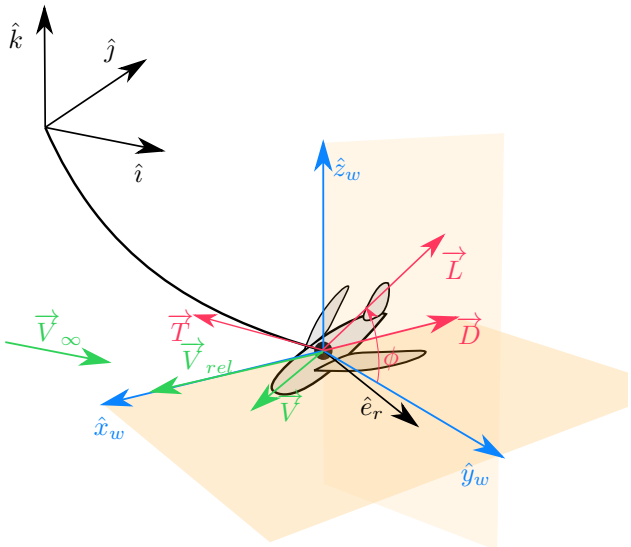

Fig. 1. Diagram of 3DOF kite, $w-$frame, and external forces

We define the position and velocity of the kite with respect to the inertial frame defined by the unit vectors $\left\{\hat{\imath}, \hat{\jmath}, \hat{k}\right\}$

$$\vec{r} = x\hat{\imath} + y\hat{\jmath} + z\hat{k} \tag{1}$$

$$\vec{V} = \dot{x}\hat{\imath} + \dot{y}\hat{\jmath} + \dot{z}\hat{k}. \tag{2}$$

We further define the position unit vector

$$\hat{e}_r = \frac{\vec{r}}{\|\vec{r}\|} \tag{3}$$

and define the relative velocity vector as

$$\vec{V}_{rel} = \vec{V} - \vec{V}_\infty \tag{4}$$

where $\vec{V}_\infty$ is the water current velocity and has the components $\{U_w, V_w, W_w\}$. We now define the w-frame (or "wind" frame) with the unit vectors $\{\hat{x}_w, \hat{y}_w, \hat{z}_w\}$ defined as

$$\hat{x}_w = \frac{\vec{V}_{rel}}{\|\vec{V}_{rel}\|} \tag{5}$$

$$\hat{z}_w = \frac{\hat{x}_w \times \hat{e}_r}{\|\hat{x}_w \times \hat{e}_r\|} \tag{6}$$

$$\hat{y}_w = \frac{\hat{z}_w \times \hat{x}_w}{\|\hat{z}_w \times \hat{x}_w\|} \tag{7}$$

We can now define the lift and drag forces the kite experiences

$$\vec{L} = \frac{1}{2}\rho C_L(\alpha) S \|\vec{V}_{rel}\|^2 (\cos\phi \hat{y}_w + \sin\phi \hat{z}_w) \tag{8}$$

$$\vec{D} = -\frac{1}{2}\rho C_D(\alpha) S \|\vec{V}_{rel}\|^2 \hat{x}_w \tag{9}$$

where $\rho, C_L, C_D, \alpha, S,$ and ϕ are respectively, the water density, the lift coefficient, the drag coefficient, the angle of attack, the wing surface, and the kite angle with respect to the $\hat{y}_w$ unit vector.

The hydrodynamic coefficients C_L and C_D are modeled in terms of α as follows::

$$C_L(\alpha) = c_1\alpha + c_2 \tag{10}$$
$$C_D(\alpha) = b_1\alpha^2 + b_2\alpha + b_3 \tag{11}$$

The sum of external forces is

$$\vec{F}_{ext} = \vec{L} + \vec{D} + \vec{T} \tag{12}$$

where $\vec{T}$ is the tension force from the tether.

We can now write a state-space model for the kite

$$\frac{d}{dt}\begin{bmatrix} x \\ y \\ z \\ u \\ v \\ w \end{bmatrix} = \begin{bmatrix} u \\ v \\ w \\ \frac{1}{m}\vec{F}_{ext}\cdot\hat{\imath} \\ \frac{1}{m}\vec{F}_{ext}\cdot\hat{\jmath} \\ \frac{1}{m}\vec{F}_{ext}\cdot\hat{k} \end{bmatrix} \tag{13}$$

where the inputs to the model are: $\{T_x, T_y, T_z, \phi, \alpha\}$.

This formulation of the kite model assumes the tension force is dictated by an additional tether model.

III. Tether Model

To explore to which extent a tether affects the dynamics of the underwater kite, we need to formulate a tether model. This model should capture the elastic behavior of the tether, and should also handle the moving boundary conditions due to both tether release and the moving kite.

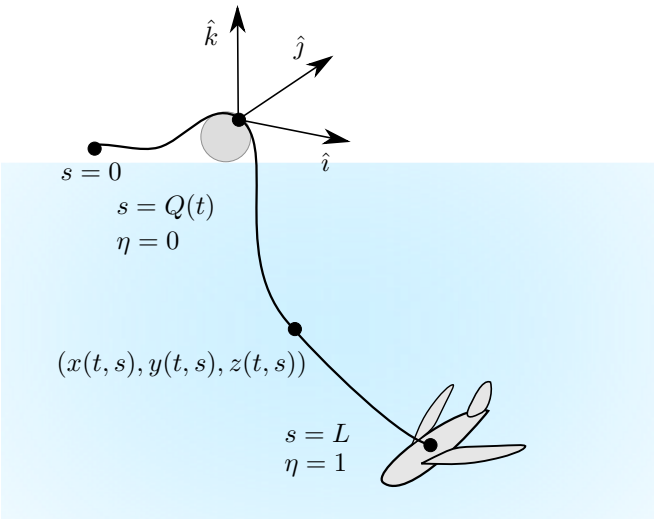

Fig. 2. Elastic tether coordinates

We define the following coordinates for the tether:

1) s: Distance along undeflected tether.
2) η: Normalized coordinate along undeflected tether.

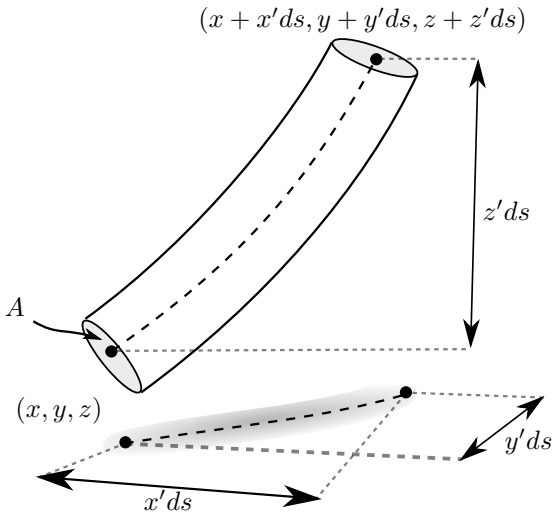

Fig. 3. Infinitesimal tether element

3) L: Total tether length.
4) $Q(t)$: Unreleased tether length.

We also define the absolute position of a point in the tether with respect to the inertial frame $\{\hat{\imath}, \hat{\jmath}, \hat{k}\}$ as: $\{x(t,s), y(t,s), z(t,s)\}$.

Now let us consider the infinitesimal element of the tether in Figure 3. We define ds as an infinitesimal change along the $s-$coordinate, and define $x' = \frac{\partial x}{\partial s}, y' = \frac{\partial y}{\partial s}, z' = \frac{\partial z}{\partial s}$.

The strain the element experiences is thus

$$\varepsilon = \frac{\sqrt{x'^2 + y'^2 + z'^2}ds - ds}{ds} \tag{14}$$

which simplifies to

$$\varepsilon = \sqrt{x'^2 + y'^2 + z'^2} - 1. \tag{15}$$

In the linear deformation region the stress the element experiences is

$$\sigma = E\varepsilon = E\sqrt{x'^2 + y'^2 + z'^2} - 1 \tag{16}$$

where E is the Young's modulus of elasticity. Given an cross-sectional area A, the tension this element experiences is

$$T = \sigma A = EA\sqrt{x'^2 + y'^2 + z'^2} - 1. \tag{17}$$

This tension acts along the tether element, with components

$$T_x = T\xi_x \tag{18}$$
$$T_y = T\xi_y \tag{19}$$
$$T_z = T\xi_z \tag{20}$$

where

$$\xi_x = \frac{x'}{\sqrt{x'^2 + y'^2 + z'^2}} \tag{21}$$

$$\xi_y = \frac{y'}{\sqrt{x'^2 + y'^2 + z'^2}} \tag{22}$$

$$\xi_z = \frac{z'}{\sqrt{x'^2 + y'^2 + z'^2}} \tag{23}$$

The dynamics of the tether can be thus described by the following system of partial differential equations

$$\ddot{x} = \frac{E}{\rho}\frac{\partial}{\partial s}\varepsilon\xi_x + \frac{q_x}{\rho} \tag{24}$$

$$\ddot{y} = \frac{E}{\rho}\frac{\partial}{\partial s}\varepsilon\xi_y + \frac{q_y}{\rho} \tag{25}$$

$$\ddot{z} = \frac{E}{\rho}\frac{\partial}{\partial s}\varepsilon\xi_z + \frac{q_z}{\rho} \tag{26}$$

where ρ is the density of the tether, and $q_{x,y,z}$ denote additional external force densities to capture, for example, buoyancy effects.

To handle the changing released tether length, we can do a coordinate transformation to the η-coordinate

$$\ddot{x} = \frac{E}{\rho(L-Q)}\frac{\partial}{\partial \eta}(\varepsilon\xi_x) + \frac{q_x}{\rho} \tag{27}$$

$$\ddot{y} = \frac{E}{\rho(L-Q)}\frac{\partial}{\partial \eta}(\varepsilon\xi_y) + \frac{q_y}{\rho} \tag{28}$$

$$\ddot{z} = \frac{E}{\rho(L-Q)}\frac{\partial}{\partial \eta}(\varepsilon\xi_z) + \frac{q_z}{\rho} \tag{29}$$

$$\dot{Q} = u(t) \tag{30}$$

Equations (27)-(30) constitute the full set of equations necessary to capture the dynamics of tether.

IV. Results

In this section we explore the effect our tether model has on the dynamics of the kite in simulations representative of a real kite system. We also explore the effect varying tether longitudinal stiffness, tether mass, and tether buoyancy have on the dynamics of the kite.

A. Inverse Dynamics Simulation

To ensure a consistent comparison between simulations, we impose a representative cross-current figure-8 trajectory in the spherical coordinates of the kite, and solve for the inputs that would yield this trajectory. We formulate this inverse dynamics problem by adding additional algebraic equations to the model presented in Section II:

$$\psi = a_1 \sin(w_1 t) \tag{31}$$

$$\theta = a_1 \sin(w_1 t)\cos(w_1 t) + \theta_0 \tag{32}$$

as well as the following differential equation:

$$\dot{r} = a_2 \sin w_2 t \tag{33}$$

where ψ and θ are the azimuth and zenith angles of the kite with respect to the floating platform.

We integrate these equation with the model through the coordinate transformation:

$$x = r\cos\psi\sin\theta \tag{34}$$

$$y = r\sin\psi\sin\theta \tag{35}$$

$$z = r\cos\theta \tag{36}$$

This trajectory, while not a power maximizing trajectory, shares the shape of the typical path tethered energy systems follow.

B. Comparison with rigid tether

We can compare the PDE tether model with a straight tether by removing the tether model and adding the additional algebraic equation:

$$\vec{T} = T\hat{e}_r \tag{37}$$

This equation captures the fact that for a straight tether, the tension always points towards the floating platform of the tether.

C. Simulation parameters

We solve the inverse dynamics problem for the straight tether and the elastic tether using the DASSL solver in OpenModelica and discretizing the PDEs along η into N segments.

All the simulations we show in this paper have the following parameters in Table I

TABLE I
SIMULATION PARAMETERS

Parameter		Value	Units
Hydrodynamic parameters:	b_1	1.221e-4	deg^{-2}
	b_2	5.309e-4	deg^{-1}
	b_3	1.1103e-2	-
	c_1	3.123e-2	deg^{-1}
	c_2	6.6675e-2	-
Kite mass:	m	100	kg
Total wing surface:	S	20	m^2
Water density	ρ	1000	kg m^{-3}
Current speed:	U_w	0.5	m s^{-2}
	V_w	0	m s^{-2}
	W_w	0	m s^{-2}
Trajectory parameters:	a_1	0.2	rad
	a_2	0.25	m s^{-1}
	w_1	0.15	rad s^{-1}
	w_2	0.1	rad s^{-1}
	θ_0	2	rad
PDE Discretization:	N	10	-

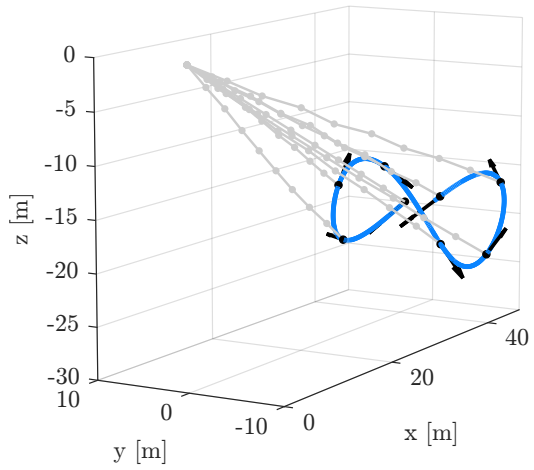

Fig. 4. Trajectory followed by the kite (in blue). Tether (grey) at different moments in time

D. Simulation comparisons

In Figure 4 we show the imposed trajectory the kite follows during the reel-out portion of the cycle.

In the simulations with a straight tether and a flexible tether the kite follows this pre-imposed figure-8 trajectory. We can thus explore the effect of having a flexible tether on the dynamics of the kite by looking at the deviations in angle of attack α and roll angle ϕ between the flexible tether simulations and the straight tether simulations.

The nominal (straight tether) input trajectories in Figures 5 and 6 are used as references for the rest of our simulations. The idea is that the more significant the effect of the tether on the kite dynamics, the larger the discrepancies between the control inputs computed by the rigid and flexible tether models.

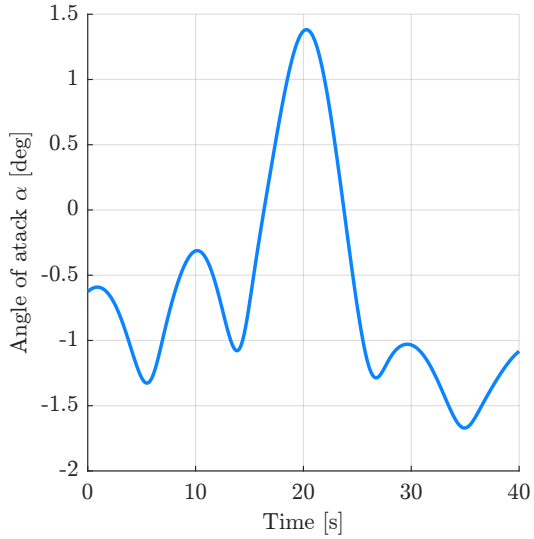

Fig. 5. Angle of attack nominal trajectory

In the rest of the figures, we explore the effect tether parameters have on the kite dynamics. We can, for instance, explore the effect of the tether mass, which we decouple from buoyancy effects by varying the radius of the tether. Figures 7 and 8 show deviations from the nominal input trajectories for three different radii.

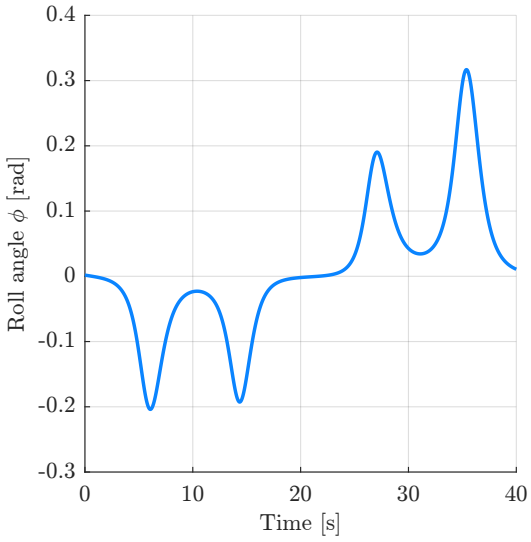

Fig. 6. Roll angle nominal trajectory

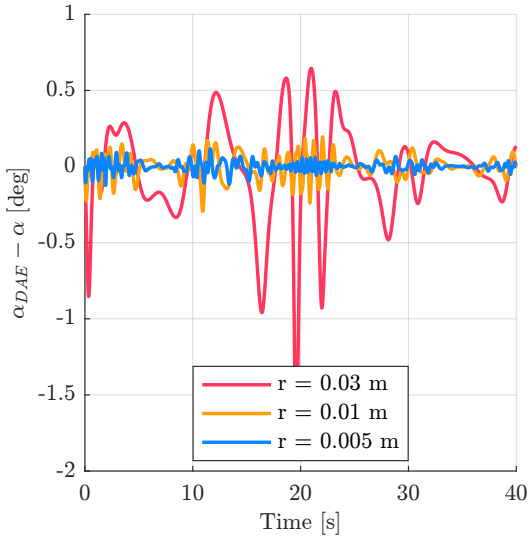

Fig. 7. Deviation from nominal angle of attack for different tether radii.

We can also explore the effect the buoyancy of the tether has on the kite. In Figures 9 and 10 we show the deviations from nominal input trajectories for different tether densities. To avoid confounding the buoyancy effect with inertial effects, we ensure the total mass of the tether is maintained constant by adjusting the radius of the tether as we change the density.

We summarize the results by looking at the root mean squared deviations of these inputs normalized by the root mean squared nominal values, in Table II.

V. Conclusion

In this paper, we explored the interplay between an elastic tether model and kite dynamics, in a marine-hydrokinetic

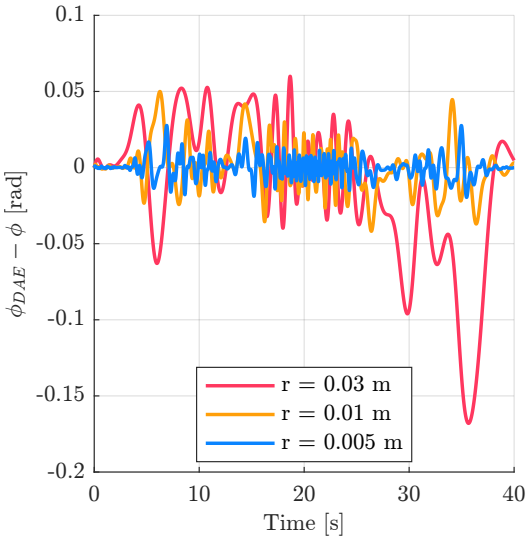

Fig. 8. Deviation from nominal roll angle for different tether radii.

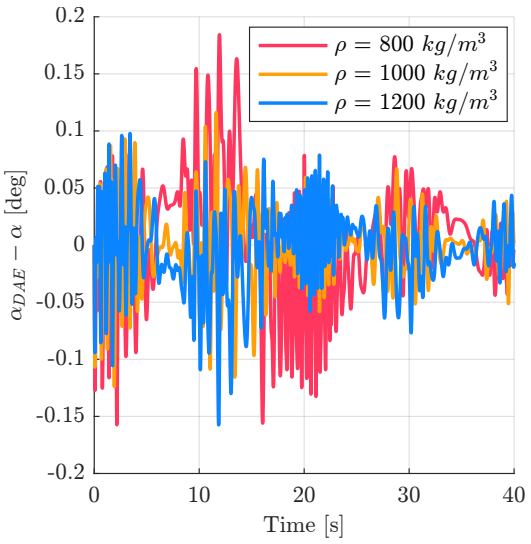

Fig. 9. Deviation from nominal angle of attack for different tether densities.

energy harvesting system. For this, a simplified model consisting of an elastic tether, and 3 degrees-of-freedom kite was developed. We compared the input trajectories of a kite following a pre-imposed representative figure-8 trajectory for a kite with an elastic tether and a kite that treats the tether as a kinematic constraint. We explored the effect of different tether parameters on the tether. Both the buoyancy of the tether and the mass of the tether required noticeable corrections of the kite inputs to track the pre-imposed trajectory. On the other hand, the longitudinal stiffness of the tether had a negligible effect. The effect of buoyancy increased for non-neutrally buoyant tethers. Particularly, the more buoyant tether with a density of $800\,\mathrm{kg\,m^{-3}}$ presented a larger normalized root mean deviation of 16 % from the nominal roll angle trajectory. The effect of mass was however the most significant of the parameters explored. For instance a $5\,\mathrm{mm}$ tether had average deviations of 7% from the nominal

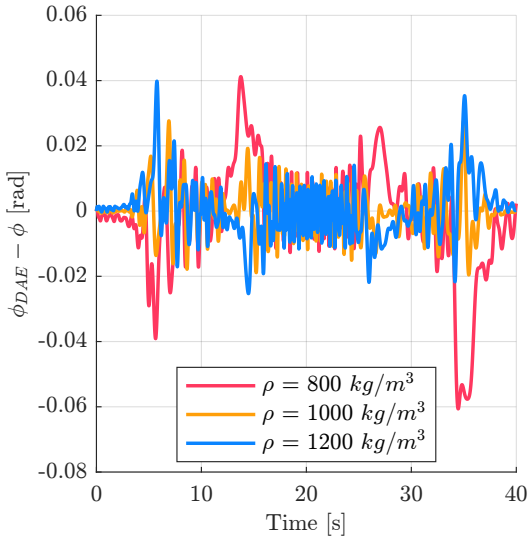

Fig. 10. Deviation from nominal roll angle for different tether densities.

TABLE II
NORMALIZED DEVIATIONS FROM NOMINAL INPUTS FOR DIFFERENT TETHER PARAMETERS

	Normalized RMSE in α	Normalized RMSE in ϕ
ρ [kg m^{-3}]		
800	0.0507	0.1601
1000	0.0304	0.067
1200	0.0324	0.0836
r [m]:		
0.005	0.0304	0.0670
0.01	0.0735	0.1586
0.03	0.3207	0.4736
E [Pa]:		
100e9	0.0304	0.0670
200e9	0.0304	0.0670

roll trajectory, while a $3\,\mathrm{cm}$ tether had average deviations of 47% from the nominal roll trajectory, meaning that it required considerably more control authority to achieve the desired figure-8 trajectory, than the kite with a massless tether.

REFERENCES

[1] J. M. Bane, R. He, M. Muglia, C. F. Lowcher, Y. Gong, and S. M. Haines, "Marine hydrokinetic energy from western boundary currents," *Annual Review of Marine Science*, vol. 9, no. 1, pp. 105–123, jan 2017.

[2] M. L. Loyd, "Crosswind kite power (for large-scale wind power production)," *Journal of Energy*, vol. 4, no. 3, pp. 106–111, may 1980.

[3] M. Cobb, K. Barton, H. Fathy, and C. Vermillion, "An iterative learning approach for online flight path optimization for tethered energy systems undergoing cyclic spooling motion." IEEE, 2019, pp. 2164–2170.

[4] H. Li, D. J. Olinger, and M. A. Demetriou, "Modeling and control of tethered undersea kites," *Ocean Engineering*, vol. 190, p. 106390, oct 2019.

[5] M. Canale, L. Fagiano, and M. Milanese, "High altitude wind energy generation using controlled power kites," *IEEE Transactions on Control Systems Technology*, vol. 18, no. 2, pp. 279–293, mar 2010.

[6] S. Costello, G. François, and D. Bonvin, "Crosswind kite control–a benchmark problem for advanced control and dynamic optimization," *European Journal of Control*, vol. 35, pp. 1–10, may 2017.

[7] P. Williams, B. Lansdorp, and W. Ockesl, "Optimal crosswind towing and power generation with tethered kites," *Journal of Guidance Control Dynamics*, vol. 31, no. 1, pp. 81–93, Jan. 2008. [Online]. Available: https://ui.adsabs.harvard.edu/abs/2008JGCD...31...81W

[8] P. Williams, B. Lansdorp, and W. Ockels, "Modeling and control of a kite on a variable length flexible inelastic tether," in *AIAA Modeling and Simulation Technologies Conference and Exhibit*. American Institute of Aeronautics and Astronautics, aug 2007.

[9] J. Koenemann, P. Williams, S. Sieberling, and M. Diehl, "Modeling of an airborne wind energy system with a flexible tether model for the optimization of landing trajectories," vol. 50, no. 1. Elsevier, jul 2017, pp. 11 944–11 950.

[10] F. Trevisi, M. Gaunaa, and M. Mcwilliam, "The Influence of Tether Sag on Airborne Wind Energy Generation," *Journal of Physics: Conference Series*, vol. 1618, p. 032006, Sept. 2020.

[11] P. Williams, P. Lapthorne, and P. Trivailo, "Circularly-towed lumped mass cable model validation from experimental data," in *AIAA Modeling and Simulation Technologies Conference and Exhibit*. American Institute of Aeronautics and Astronautics, aug 2006.

[12] A. Siddiqui, K. Naik, M. Cobb, K. Granlund, and C. Vermillion, "Lab-scale, closed-loop experimental characterization, model refinement, and validation of a hydrokinetic energy-harvesting ocean kite," aug 2020.

[13] C. M. Ablow and S. Schechter, "Numerical simulation of undersea cable dynamics," *Ocean Engineering*, vol. 10, no. 6, pp. 443–457, jan 1983.

[14] F. R. Driscoll, R. G. Lueck, and M. Nahon, "Development and validation of a lumped-mass dynamics model of a deep-sea rov system," *Applied Ocean Research*, vol. 22, no. 3, pp. 169–182, jun 2000.